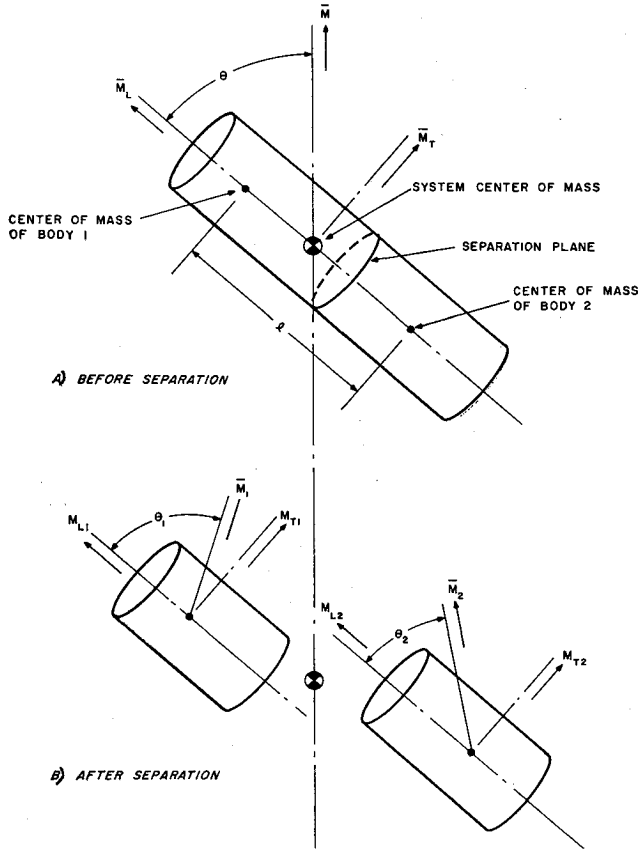

Fig. 1 Vector diagram.

in Fig. 1, the angular momentums about the longitudinal and transverse axes prior to separation are

$$M_L = (I_{L_1} + I_{L_2} + \mu l^2)\omega_l \tag{1}$$

$$M_T = (I_{T_1} + I_{T_2})\omega_t \tag{2}$$

The coning angle is defined as

$$\tan\theta = \frac{M_T}{M_L} = \left(\frac{I_{T_1} + I_{T_2}}{I_{L_1} + I_{L_2} + \mu l^2}\right)\frac{W_t}{W_l} \tag{3}$$

Immediately after separation and assuming a perfect separation mechanism, the components of angular momentum of m_1 about its own center of mass are

$$M_{L_1} = I_{L_1}\omega_{l_1} \tag{4}$$

$$M_{T_1} = I_{T_1}\omega_{t_1} \tag{5}$$

But $\omega_{l1} = \omega_l$ and $\omega_{t1} = \omega_t$, since in the process of separation no external torques were introduced. The coning angle for m_1 is

$$\tan\theta_1 = I_{T_1}\omega_t / I_{L_1}\omega_l \tag{6}$$

In a similar manner,

$$M_{L_2} = I_{L_2}\omega_l \tag{7}$$

$$M_{T_2} = I_{T_2}\omega_t \tag{8}$$

$$\tan\theta_2 = (I_{T2}/I_{L2})(\omega_t/\omega_l) \tag{9}$$

Angular momentum of the system is conserved by the motion of m_1 and m_2 about the system center of mass. The coning angle of the payload after separation is increased or decreased over that of the configuration before separation according to the relationship

$$\frac{L_{T_1}}{I_{L_1}} \gtreqless \frac{I_{T_1} + I_{T_2}}{I_{L_1} + I_{L_2} + \mu l^2} \tag{10}$$

which can be written as

$$0 \gtreqless \frac{I_{T_2}}{I_{T_1}} - \frac{I_{L_2}}{I_{L_1}} - \frac{\mu l^2}{I_{L_1}} \tag{11}$$

Similar relationships are true for the booster coning angle. It is, therefore, possible for the coning angle of the payload to increase or decrease even with a perfect separation mechanism.

Choosing Optical Properties of Noncharring Ablators

LAWRENCE E. HOOKS*
Air Force Systems Command,
Wright-Patterson Air Force Base, Ohio

Nomenclature

a = attenuation coefficient
E = σT^4
$\dot{m}$ = mass ablation rate per unit area
q^* = ablation parameter
r = flake reflectivity
T = absolute temperature
σ = Stefan-Boltzmann constant

Subscript
A = ablation

THE noses of superorbital re-entry vehicles will receive significant radiant heating pulses during deceleration to orbital speeds. Designers of such vehicles must prevent this energy from penetrating to the load-bearing structures. This may be done by using opaque heat shields, charring ablators, or ablators that have opaque vapor states. Discussing transparent, noncharring ablators with transparent vapor states, Allen[1] suggests another way to prevent radiation penetration: add metal flakes to the heat shield, orienting these flakes to reflect gas cap radiation away from the vehicle.

This note develops the ablation rate expression for a transparent ablator and simplifies the expression for two conditions: negligible radiant heating and substantial radiant heating. The transparent ablator is compared to an opaque ablator on the basis of minimum ablation rate for the two radiant heating conditions.

Assuming that the first metal flakes in the transparent ablator are located parallel to the shield surface at a depth L and that thermal conduction is negligible in the surface layer of depth L (L layer), the power balance for an elemental area of the L layer and the flake may be written as

$$q_{ci} + q_{Ri} = q_A + q_\epsilon + q_{R0} \tag{1}$$

where q_{ci} is convective heat flux in, q_{Ri} is flux in due to gas cap radiation, q_A is flux carried away by vaporized ablator, q_ϵ is thermal emission from the L layer and the flake, and q_{R0} is unabsorbed gas cap radiation leaving the area element after reflection from the flake.

The net heating into the skin element is

$$q_{Ni} = q_{ci} + q_{NR} = q_A + q_\epsilon \tag{2}$$

where $q_{NR} \equiv q_{Ri} - q_{R0}$ is the net radiant energy absorbed by the L layer and the flake. Now,

$$q_A \equiv q^*\dot{m} \tag{3}$$

Received June 13, 1963; revision received August 19, 1963. The author thanks W. L. Hankey Jr. for his aid during preparation of this note.

* Physicist, Air Force Flight Dynamics Laboratory, Research and Technology Division.

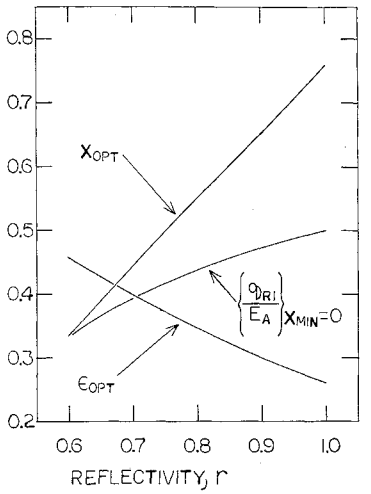

Fig. 1 Transparent ablator properties.

Solving Eqs. (2) and (3) for $\dot{m}$,

$$\dot{m} = (1/q^*)\{q_{ci} + q_{NR} - q_\epsilon\} \tag{4}$$

The variation of $\dot{m}$ with $x(\equiv aL)$, the attenuation factor of the L layer, is

$$\frac{\partial \dot{m}}{\partial x} = \frac{1}{q^*}\left\{\frac{\partial q_{NR}}{\partial x} - \frac{\partial q_\epsilon}{\partial x}\right\} \tag{5}$$

To evaluate $\dot{m}$ and $\partial\dot{m}/\partial x$, q_ϵ and q_{NR} must be obtained as functions of x.

Assuming that attenuation coefficient and temperature are constant in the L layer and that the area element is two-dimensional,

$$q_\epsilon = \tfrac{1}{2}x\,E_A \exp(-x) + \tfrac{1}{2}rx\,E_A \exp(-2x) + (1-r)E_A \exp(-x) \tag{6}$$

The first right-hand term is power radiated directly to the external surface from the volume of the L layer. The second term is volume-radiated power that reaches the L layer-flake interface and is then reflected from the flake to the external surface. The $\exp(-x)$ in the first term and one $\exp(-x)$ factor of $\exp(-2x)$ in the second term approximate the attenuation of isotropic bulk radiation from an infinite slab before it reaches one slab face. This model was chosen by inspecting the more exact model formed by inserting the absorption factor $\exp(-ar)$ in the integral given by Yoshikawa and Wick[2] for an analogous situation (r means radial distance here).

The second $\exp(-x)$ factor in the second term and the $\exp(-x)$ in the third term represent the attenuation of a beam of radiation passing through a slab from surface to surface (Lambert's law). In the second term, the impinging beam intensity is $\frac{1}{2}rxE_A \exp(-x)$, the bulk radiation reflected from the flake. In the third term, the impinging beam intensity is $(1-r)E_A$, the radiant flux emitted by the flake. The two $\exp(-x)$ factors used next in Eq. (7) are beam attenuation terms.

The gas cap radiation entering the area element is reduced by $\exp(-x)$ when it reaches the flake, r of the remaining power is reflected, and $\exp(-x)$ of the reflected power reaches the shield surface again. This gives

$$q_{R0} = q_{Ri}\, r \exp(-2x) \tag{7}$$

Inserting Eqs. (6) and (7) in Eqs. (4) and (5),

$$\dot{m} = (1/q^*)[q_{ci} + (1 - re^{-2x})q_{Ri} - \{(x/2) + (rx/2)e^{-x} + (1-r)\}\, e^{-x}E_A] \tag{8}$$

$$\partial\dot{m}/\partial x = (1/q^*)[2re^{-2x}\, q_{Ri} - \{2r + re^{-x}(1-2x) - (1+x)\}(e^{-x}/2)E_A] \tag{9}$$

Three general statements on the properties of semitransparent materials backed by reflectors may be deduced from Eqs. (8) and (9):

1) Absorptivity, $\{1 - r\exp(-2x)\}$, is not equivalent to emissivity, $[\{x/2 + (rx/2)\exp(-x) + (1-r)\}\exp(-x)]$, although it may be numerically equal for special values of x and r.

2) There is an x value for each r for which emissivity is a maximum (x_{opt}). This is also the x value for which $\dot{m}$ is a minimum when $q_{Ri}/E_A \approx 0$ (mathematically, $q_{Ri} = 0$). Figure 1 shows x_{opt} vs r.

3) For increasing q_{Ri}/E_A, the x value for minimum $\dot{m}$ decreases. Figure 1 shows q_{Ri}/E_A vs r for which this x_{min} reaches zero. Note that x_{min} and x_{opt} are not the same for $q_{Ri}/E_A \neq 0$, since x_{min} depends on both absorptivity and emissivity, whereas x_{opt} depends only on emissivity. For values of q_{Ri}/E_A greater than those shown in Fig. 1, the x value for minimum $\dot{m}$ is always equal to zero.

Will q_{Ri}/E_A values greater than those in Fig. 1 occur in flight situations of interest? Consider a point on a lifting superorbital re-entry trajectory: 35 kft/sec, 200 kft. Let the nose radius be 1 ft, and let T_A be 2460°R. For these conditions, $q_{Ri} = 50$ Btu/ft²-sec,[3] and $E_A = 36.5$ Btu/ft²-sec.[4] $q_{Ri}/E_A \geq 1.37$ here, since the preceding q_{Ri} is for an equilibrium shock layer and is thus a lower limit.

For $x \approx 0$ with $q_{Ri}/E_A > 0$,

$$\dot{m} \approx (1/q^*)\{q_{ci} + (1-r)q_{Ri} - (1-r)E_A\} \tag{10}$$

and for $q_{Ri}/E_A \approx 0$, with $x = x_{opt}$,

$$\dot{m} \approx (1/q^*)\{q_{ci} - \epsilon_{opt}E_A\} \tag{11}$$

where ϵ_{opt} is the ϵ corresponding to x_{opt}; ϵ_{opt} is displayed in Fig. 1. Note that large r decreases $\dot{m}$ for q_{Ri}/E_A large, whereas Fig. 1 shows that small r will decrease $\dot{m}$ for $q_{Ri}/E_A \approx 0$. Treating the reflector as an opaque material for which emissivity and absorptivity are equivalent, reducing emissivity reduces $\dot{m}$ for large q_{Ri}/E_A, whereas increasing emissivity reduces $\dot{m}$ for $q_{Ri}/E_A \approx 0$.

Next, consider an opaque ablator with variable emissivity (therefore, noncharring). Assuming that emissivity and absorptivity are equivalent for this ablator, the power balance equation corresponding to Eq. (1) is

$$q_{ci} + \epsilon q_{Ri} = q_A + q_\epsilon \tag{12}$$

setting $q_\epsilon = \epsilon E_A$,

$$\dot{m} = (1/q^*)\{q_{ci} + \epsilon q_{Ri} - \epsilon E_A\} \tag{13}$$

For this type of ablator, decreasing ϵ decreases $\dot{m}$ when $q_{Ri}/E_A > 1$. Increasing ϵ decreases $\dot{m}$ when $q_{Ri}/E_A < 1$.

Writing $1 - r = \epsilon$ in Eq. (13) and comparing that with Eq. (10), it is seen that $\dot{m}$ is the same for the transparent ablator with flakes and the opaque ablator when r is the same. For $q_{Ri}/E_A \approx 0$, a comparison of Eqs. (11) and (13) shows that $\dot{m}$ may be made less for the opaque ablator than for the transparent ablator, since emissivities greater than ϵ_{opt} may easily be achieved for opaque ablators.

Consideration of the practical difficulties in creating a transparent ablator with small flakes embedded in it (parallel to each other and spaced so that x is both small and relatively constant as ablation progresses) suggests that opaque ablators are more usable for $q_{Ri}/E_A > 1$, for which the semitransparent and opaque ablators have equal $\dot{m}$.

This note shows that Allen's basic idea, i.e., reflecting shock-layer radiation rather than absorbing it, is a valid technique for reducing $\dot{m}$ at those trajectory points and those vehicle surface areas for which $q_{Ri}/E_A > 1$. An opaque ablating heat shield designed according to the criterion developed here for a superorbital re-entry craft would have the following characteristics. An outer layer of high emissivity ablator would receive the initial superorbital convective heating. As q_{Ri}/E_A increased through one, the high emissivity layer would be removed by ablation to present a highly reflective

ablator surface. The highly reflective surface would receive the radiant heating peak of the superorbital re-entry and give way to another high-emissivity layer as q_{Ri}/E_A decreased through one.

References

[1] Allen, H. J., "Gas dynamics problems of space vehicles," NASA SP-24, pp. 1–17 (1962).

[2] Yoshikawa, K. K. and Wick, B. H., "Radiative heat transfer during atmosphere entry at parabolic velocity," NASA TN D-1074, p. 6 (1961).

[3] "Aerodynamic heat transfer handbook," Vol. I, Boeing Airplane Co. D2-9514, Sec. 5, 4, 15 (1960).

[4] Hankey, W. L., Jr., Neumann, R. D., and Flinn, E. H., "Design procedures for computing aerodynamic heating at hypersonic speeds," Wright Air Dev. Center TR 59-610, p. 100 (1960).

Real-Gas Hypersonic Blunt-Body Flows

Rudolph J. Swigart*

Lockheed Missiles and Space Company, Huntsville, Ala.

Introduction

Several accurate methods have been developed for analyzing inviscid hypersonic flows around blunt bodies (see, e.g., Refs. 1–3). In most of these methods, however, the gas is assumed to be perfect, i.e., one that obeys the equation of state $p = \rho RT$, where p is the pressure, ρ the density, R the gas constant, and T the temperature, and has a constant ratio of specific heats. The use of such a state equation is well justified in that accurate results are obtained at flight Mach numbers for which molecular vibration, dissociation, and ionization in the flow between the detached bow shock wave and the body is nonexistent or negligibly small. However, as the flight Mach number and hence temperature behind the shock increases, the vibrational energy modes become excited and the gas begins to dissociate and ionize. Upon excitation of the vibrational energy modes, the specific-heat ratio no longer remains constant, and, with the onset of dissociation, the relation $p = \rho RT$ becomes inaccurate. Thus, although perfect-gas results for flight Mach numbers above those at which real-gas effects become significant still yield important qualitative features of the flow field, quantitative accuracy of thermodynamic and physical variables decreases.

In order to increase the accuracy of existing inviscid equilibrium perfect-gas blunt-body solutions at flight Mach numbers above those at which real-gas effects become important, several investigators have modified perfect-gas solutions to handle real-gas effects. The Research and Advanced Systems Branch of the Aero and Propulsion Sciences Group at Norair Division of the Northrop Corporation has developed an equilibrium real-gas solution[4] in which the perfect-gas equation of state is replaced by Hansen's[5] closed-form expressions for the thermodynamic properties of equilibrium air. Van Dyke's[6] method of numerical integration of partial differential equations is used by the Northrop group. Lomax and Inouye[7] of NASA-Ames have developed a solution combining the equilibrium-air data of Hilsenrath and Beckett[8] with the Van Dyke Solution.†

Received July 2, 1963; revision received September 16, 1963.

* Associate Research Scientist, Huntsville Research and Engineering Center.

† This work of Lomax and Inouye is unpublished to date. Some of the results were made available to the author and are used in this note for comparison purposes.

For real-gas solutions such as developed at Northrop and Ames, a substantial amount of labor is required to incorporate the real-gas equations of state into the basic solution. Hansen's expressions for the thermodynamic properties are lengthy, and the NASA solution requires computing machine storage of the Hilsenrath and Beckett tables, along with table look-up and interpolation routines. Hence, it would be advantageous if an approximate equilibrium real-gas thermodynamic description could be developed that, when used to replace perfect-gas thermodynamics in any accurate blunt-body solution, would yield accuracy to within a few percent of the more exact solutions at only a fraction of the labor.

By assuming the equilibrium real-gas flow between the shock and a blunt-nosed body to be one of constant specific-heat ratio different from the undissociated freestream value, an approximate equilibrium real-gas thermodynamic description is obtained. The author's blunt-body method[9] is modified to accommodate the approximate thermodynamic description of the actual equilibrium real-gas flow. Results are compared with those obtained at Northrop and Ames, and also with perfect-gas solutions.

Approximate Equilibrium Real-Gas Thermodynamics

As previously mentioned, the equilibrium real-gas flow between the shock wave and body is assumed to be one of constant specific-heat ratio. In addition, this gas is assumed to obey the equation of state

$$h = [\gamma/(\gamma - 1)](p/\rho) + \tilde{A} \tag{1}$$

where h is the enthalpy, p the pressure, $\tilde{A}$ a constant, and γ the adiabatic index defined by

$$\gamma = (\partial \ln p/\partial \ln \rho)_s = a^2\rho/p \tag{2}$$

where s is the entropy and a the speed of sound. The assumption of Eq. (1) for the equation of state in the shock layer can be given physical justification by noting that it is tantamount to assuming that each species in the shock layer behaves as a perfect gas having the same ratio of specific heats, γ. The constant $\tilde{A}$ is then identifiable with the dissociation-energy contribution to the enthalpy.

By use of the Second Law of Thermodynamics it can be proven that, for a gas having the state equation, Eq. (1), the entropy s is a function of p/ρ^γ only. Thus, since entropy is conserved along streamlines in equilibrium flow, introduction of a stream function into the governing equations of fluid mechanics yields

$$p/\rho^\gamma = g(\psi) \tag{3}$$

where ψ is the stream function and the functional form of g is determined from the boundary conditions at the shock wave. Then, modification of an accurate blunt-body solution such as that of Van Dyke[1] or Swigart[9] reduces to modification of the shock-wave boundary conditions and the function $g(\psi)$. For the real-gas description under consideration, the density ratio across the shock wave becomes

$$\frac{\rho_s}{\rho_\infty} = \left\{\frac{\gamma}{\gamma+1}\left[1 + \frac{1 - B\xi^2}{\gamma_\infty M^2(1 + C\xi^2)}\right] - \frac{\gamma}{\gamma_\infty(\gamma+1)M^2} \times \left[\left(\frac{1 + C\xi^2}{1 - B\xi^2}\right)^2 + \left(\frac{\gamma_\infty}{\gamma}\right)^2 M^4\left(\frac{2\gamma^2}{\gamma_\infty M^2} - 2(\gamma^2 - 1) \times \left\{\frac{1}{(\gamma_\infty - 1)M^2} - A\right\}\right)\left(\frac{1 + C\xi^2}{1 - B\xi^2}\right) + \left(\frac{\gamma_\infty}{\gamma}\right)^2 M^4\right]^{1/2}\right\}^{-1} \tag{4}$$

where B is a parameter characterizing the shock-wave shape,[6,9] $C = 1 - B$, ξ is distance along the shock, M is the freestream Mach number, $A = \tilde{A}/q_\infty^2$, where q_∞ is the freestream speed, and γ_∞ is the specific-heat ratio in the freestream. The